Compressed hydrides as metallic hydrogen superconductors

Yundi Quan, Soham S. Ghosh, and Warren E. Pickett

Compressed Hydrides as Metallic Hydrogen Superconductors

Yundi Quan, Soham S. Ghosh, and Warren E. Pickett

University of California Davis, Davis CA 95616[*]

(Dated: October 14, 2019)

The 2014-2015 prediction, discovery, and confirmation of record high temperature superconductivity above 200K in compressed H_3S, followed by the 2018 extension to superconductivity in the 250-260K range in lanthanum hydride, marks a new era in the longstanding quest for room temperature superconductivity: quest achieved, at the cost of supplying 1.5-2 megabars pressure. Predictions of numerous high temperature superconducting metal hydrides XH_n (X=metal atom) have appeared, but are providing limited understanding of why some transition temperatures T_c are high while others are low. We make use of the small mass ratio M_H/M_X to obtain an atomic decomposition of the coupling strength to reveal that although the X atom provides coupling strength via λ_X as commonly calculated, it is irrelevant for T_c because the resulting lowering of frequency moments compensates (and sometimes over-compensates) for the increase in λ. It is important for analysis and for understanding that the X atom contribution is *neglected*, because T_c depends more transparently on λ_H. Five XH_n compounds, predicted in harmonic approximation to have T_c in the 150-300K range, are analyzed consistently for their relevant properties, revealing some aspects that confront conventional wisdom. A phonon frequency – critical temperature (ω_2-T_c) phase diagram is obtained that reveals a common structural phase instability boundary limiting T_c at the *low pressure* range of each compound. The hydrogen scattering matrix elements are obtained and found to differ strongly over the hydrides. A quantity directly proportional to T_c in these hydrides is identified, indicating that (in common notation) $N_H(0)I_H^2/\omega_H = \eta_H/\omega_H$ is the parameter combination to be maximized in hydrides.

PACS numbers:

I. BACKGROUND

The disruptive discovery of record high temperature superconductivity (HTS) in SH_3 above 200K[1–4] has now been superseded by reports from two groups of critical temperatures T_c in the 250-260K range in lanthanum hydride,[5–7] both requiring pressure in the 160-190 GPa range. Even more recently, T_c up to 240K has been report in yttrium hydrides.[8] The mechanism of pairing is convincingly electron-phonon coupling (EPC) in these hydrides,[1, 9–15], and several predictions of HTS in dozens of other metal hydrides at high pressure have appeared, see for example [4, 9, 16–23]. For prediction of new superconductors it is essential to identify the energetically favorable structures and there has been an emphasis on this issue in several of these studies.[1, 4, 9, 11, 12, 14, 16–22] However, relatively little has been decided about the relative importance of the few underlying characteristics that determine T_c. This issue of analysis and understanding of the microscopic mechanisms is the topic of this paper.

For EPC superconductivity, the critical temperature T_c is determined by a retarded Coulomb repulsion μ^*, a minor property that varies only within the range 0.10-0.15, and the function of primary interest, the Eliashberg EPC spectral function $\alpha^2F(\omega) = \alpha^2(\omega)F(\omega)$, where $F(\omega)$ is the phonon density of states and $\alpha^2(\omega)$ gives the coupling strength from phonons of frequency ω. While calculating (or measuring) α^2F is essential for any basic understanding of the coupling, T_c itself can be obtained sufficiently accurately from the Allen-Dynes equation[24] $T_c = T_c^{AD}(\lambda, \omega_{log}, \omega_2; \mu^*)$ in terms of the EPC coupling strength λ and two frequency moments obtained from α^2F, the logarithmic ω_{log} and second ω_2 frequency moments. Specific expressions are provided in the Supplemental Material (SM).[25] For all aspects of the EPC formalism and implementation, the review of Giustino can be consulted.[26] A useful review of methods and materials for conventional high temperature superconductors has been provided by Flores-Livas *et al.*[27]

Compounds present challenges in obtaining the relative importance of the various constituent

[*]Electronic address: `wepickett@ucdavis.edu`
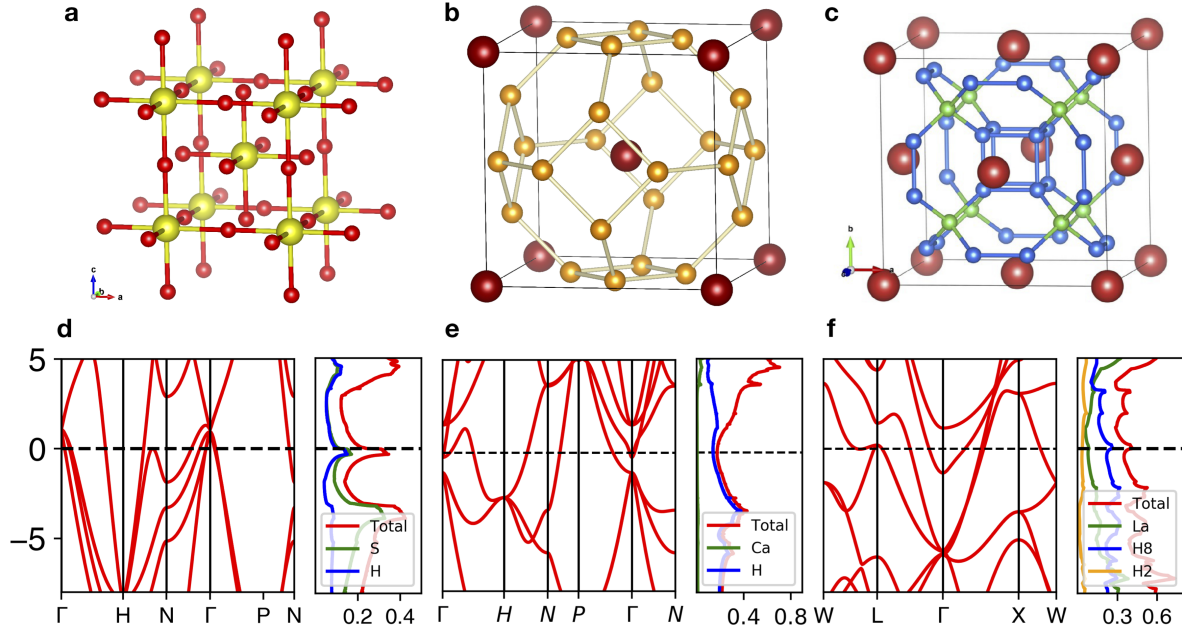
FIG. 1: Top row: crystal structures of $n=3$ bcc SH$_3$, of $n=6$ bcc CaH$_6$, and $n=10$ fcc LaH$_{10}$. Lower row: corresponding band structures (in eV) and electronic densities of states (in states/eV-unit cell). In each case several bands cross the Fermi level.

atoms. With λ given by

$$\lambda = \int \frac{2}{\omega} \alpha^2 F(\omega) d\omega \rightarrow \frac{N(0)I^2}{M\omega_2^2}, \qquad (1)$$

individual atomic contributions are spread throughout $\alpha^2(\omega)$ and $F(\omega)$. For an elemental metal, one has the exact decomposition given at the right side of Eq. 1 in terms of the Fermi level ($E_F = 0$) density of states $N(0)$, the Fermi surface averaged squared electron-ion matrix element I^2, the atomic mass M, and the second moment ω_2. The scattering strength is given by the change in crystal potential $V(\vec{r})$ due to the displacement of the atom at $\vec{R}$

$$I^2 = \left\langle \left\langle | < k | \frac{dV}{d\vec{R}} | k' > |^2 \right\rangle \right\rangle_{FS}, \qquad (2)$$

where the large brackets indicate a double average of $\vec{k}, \vec{k}'$ over the Fermi surface.

In generic compounds no such decomposition to atomic values is possible, because the more general expression for the Fermi surface averaged matrix elements in Eq. 2 depends on displacement of

pairs of distinct atoms. A main point of this paper is that for binary hydrides XH_n, atom-specific (subscript $j = X, H$) values

$$\lambda_j = N_j(0)I_j^2/M_j\omega_{2,j}^2, \quad \lambda = \lambda_X + \lambda_H. \qquad (3)$$

can be obtained with great accuracy and applied to great advantage to understand the origins and possible limits of T_c. The three crystal classes encompassing five hydrides that we have studied and compared are illustrated in Fig. 1.

II. ATOMIC ANALYSIS: H VERSUS METAL ATOM X

Binary hydrides provide a unique opportunity: the light mass of H results in separation of the phonon spectrum $\omega_{q,\nu}$ and $F(\omega)$ into disjoint metal atom low frequency, and H high frequency, regimes, with examples given below. One thus obtains separate $\alpha^2 F_j(\omega)$ functions for each atom type $j=X$ or H from the associated frequency regime, and consequently for $\lambda = \lambda_X + \lambda_H$ as well. Reported predictions for XH_n compounds

2

often quote the X and H contributions to λ separately.

This separation provides the extension to specific atomic contributions λ_j at the right side of Eq. 1. The subscript refers to each atom type j; $N_j(0)$ is the atom-type projected electronic DOS and the other quantities are evident. Since λ, its denominator, and $N_j(0)$ are all known after calculation, we can for the first time extract the atom-specific Fermi surface averaged matrix elements I_j^2 for each atom type in a compound, because these squared matrix elements contain cross-terms from pairs of distinct atoms. Specifically, we obtain I_H^2 for each hydride for comparison. In addition, H frequency moments that are uncontaminated by X contributions are obtained, for comparison across the hydrides.

We first note that from Eq. 3 it seems crucial for high pressure superconductivity that I_j^2 *increases with pressure* comparably to $M_j\omega_{2,j}^2$, to maintain if not to increase λ_j and λ. The behavior of the atom specific I^2 in metals is almost unexplored in compounds, the exception being some insight obtained from the rigid atomic potential model,[28–30] which has been applied successfully to close packed medium temperature (former high temperature) superconductors. While all the contributions to I_j^2 are available from modern EPC codes, the information has never been extracted and exploited for a deeper understanding of screening of the proton motion and its impact on high T_c.

The importance of I^2 is evident as it is one of the three components of $\lambda_j = \eta_j/\kappa_j$: $\eta_j = N_j(0)I_j^2$, and $M_j\omega_{2,j}^2 \equiv \kappa_j$. κ_j is the effective harmonic *lattice stiffness* constant for atom j, thus the McMillan-Hopfield[31, 32] parameter $\eta_j = N_j(0)I_j^2$ is an effective *electronic stiffness* for atom j, and $\lambda_j = \eta_j/\kappa_j$ is their ratio. The strong coupling limit explored by Allen and Dynes[24] gives $T_c \rightarrow 0.18\sqrt{\eta/M} = 0.18\sqrt{N(0)I^2/M}$, further emphasizing the importance of I^2 along with $N(0)$ and M, also indicating the seeming *irrelevance of frequencies*. For these hydrides, we obtain a linear relation between T_c and H (not total) parameters, discussed later.

To extract these various quantities from published papers in which often only limited information is provided, we describe in the SM[25] a constrained model[10] of a piecewise constant α^2F that enables extraction from published figures, information of the type that we introduce in this paper.

III. CRYSTAL STRUCTURE AND METHODS

In Fig. 1 the bcc $Im\bar{3}m$ space group structure of SH_3, the fcc $Fm\bar{3}m$ structure of LaH_{10}, which has two hydrogen sites H2 (green) and H8 (blue) with two and eight sites respectively, and the bcc XH_6 structure are shown. (For structural information see the SM.[25]) An overview of the electronic band structure and atom-projected density of states (DOS) are also shown. Several bands cross the Fermi energy (the zero of energy) so the detailed band structure *per se* provides little useful information about superconductivity. The LaH_{10} 1:10 stoichiometry is calculated to be dynamically stable in the observed pressure range and the La sublattice has been observed to be fcc,[6] making it the candidate structure of choice for the recent signals of superconductivity in La-H samples in the 250-280K range.[5–7] From one viewpoint, the La atom sits inside a hydrogen cage of 32 H atoms, as shown in Fig. 1, prompting the description as a clathrate structure.

Electronic structure calculations were carried out using the pseudopotential (PP) Quantum Espresso (QE) code.[33] We have found that the results can be sensitive to the choice of PP, which partially accounts for the differing results that can be found in the literature for certain compounds. We have conservatively and consistently used Hamann's optimized norm-conserved Vanderbilt PPs identified as *oncv* pseudopotentials.[34] The energy cutoffs for wave function and charge density expansion are 80 Ry and 480 Ry respectively.

For self-consistent calculations, a mesh of $24\times24\times24$ k points is used. The generalized gradient approximation[35] was adopted for the exchange-correlation functional. The optimized tetrahedron method, as implemented by Kawamura *et al.* in QE, is used for Brillouin zone integration.[36] The dense mesh that we have used provides accurate energy resolutions of $N(E)$ when van Hove singularities fall at E_F, as occurs in both SH_3 and LaH_{10}. For phonon dispersion calculations, the $6\times6\times6$ q-mesh includes the Γ point, while to obtain electron-phonon coupling from the optimized tetrahedron method, we used a similar mesh that is displaced from Γ. Since these com-

pounds are three dimensional, they do not display Kohn anomalies (rare in 3D). Also, they have strong metallic screening, so the interatomic forces constants will be relatively short range. Because of these factors, the phonon dispersion dispersion curves are rather smooth, and dense q sampling is not required for the trends with pressure that we are exploring.

Anharmonic corrections are known to be important for phonons and thereby T_c in both SH_3 and LaH_{10}, and to stabilize them to lower pressures.[11, 37] Quantum fluctuations of the H atom arise in SH_3[14] and can shift boundaries in the phase diagrams.[38] In this study we restrict ourselves to the harmonic approximation and neglect quantum fluctuations; these effects shift phase diagram boundaries but do not impact our conclusions. Only with these simplifications do the formal expressions for EPC apply. We calculate the electronic and phononic spectra, electron-phonon coupling and $\alpha^2 F$ using the EPW (Electrons and Phonons with Wannier functions) code,[39, 40] and use the Coulomb repulsion constant $\mu^* = 0.13$ throughout.

T_c is calculated consistently for all compounds from the full Allen-Dynes equation, which is a refitting to dozens of calculations to an extension of the McMillan equation for T_c to include (very) strong coupling and phonon-spectrum-shape corrections. The full expression, which sports a prefactor of the logarithmic moment ω_{log} as a primary feature, is provided in the SM.[25]

IV. NEW BEHAVIOR HOLDING ACROSS THE HYDRIDES

The compounds we discuss – SH_3; CaH_6 and MgH_6; LaH_{10} and YH_{10} – share broad features: they have cubic symmetry, they have a single X atom per primitive cell, and many bands cross E_F (see Fig. 1 for crystal structures and band structures), giving a multisheeted Fermi surface, the details of which do not seem to be important except for the possible occurrence of vHs.[15] At the high pressures, lying variously across 160-400 GPa across this study, for which these structures have been reported (calculated) to be harmonically stable, the H vibrations dominate the optic modes with energies up to 220-250 meV, which are distinct from the X dominated acoustic modes at 70 meV or lower, depending on the X atom mass. Ta-

bles I-III in the Appendix contains the materials parameters obtained from our studies. The main results are as follows.

A. The dominance of hydrogen

The anticipated importance of H for T_c in hydrides is clouded by the observation that the X atom provides 15-25% of λ, seemingly very important. An overriding feature in our results of the tables in the Appendix is that coupling λ_X from the metal atom is useless in increasing T_c, at best enhancing T_c by only 3% although the total λ is increased by the above mentioned 15-25%. More startlingly, including the X portion of $\alpha^2 F$ can *decrease* T_c. For example, for LaH_{10} at both 250 and 300 GPa, including λ_X increases λ by +14%, but this increased strength at low frequency *decreases* ω_{log} by 18% producing a net *decrease of T_c* by 5%. λ_X thus becomes a source of misconceptions, and by being included in obtaining T_c as in previous calculations, it has resulted in an impression (incorrect) that it contributes proportionally to T_c.

This anti-intuitive behavior appears to contradict the result of Bergmann and Rainer[41] that any small increase in coupling increases T_c, that is, $\delta T_c / \delta \alpha^2 F(\omega)$ is non-negative. The resolution of this conundrum lies in effects that have been addressed before:[42–44] in physical materials (and in a self-consistent treatment) an increase in $\alpha^2 F$ at a given frequency will feed back into a softening of phonon modes. This mode softening always opposes the positive effect on T_c from the increase in λ. For X=La in LaH_{10} the softening dominates, and (as mentioned) T_c *drops by 5%* in spite of stronger coupling, just before the lattice instability sets in (see below). T_c in CaH_6 and MgH_6 is effectively unchanged under the 15-20% increase from λ_X; SH_3 shows a small positive effect. The important message is that for T_c, λ_X is ineffectual and it should be disregarded to gain knowledge about increasing T_c. This option is included in the tables in the Appendix.

B. Our major results

Since it was just established that X atom coupling is ineffective at best and misleading in practice, henceforward we focus on the H atom contri-
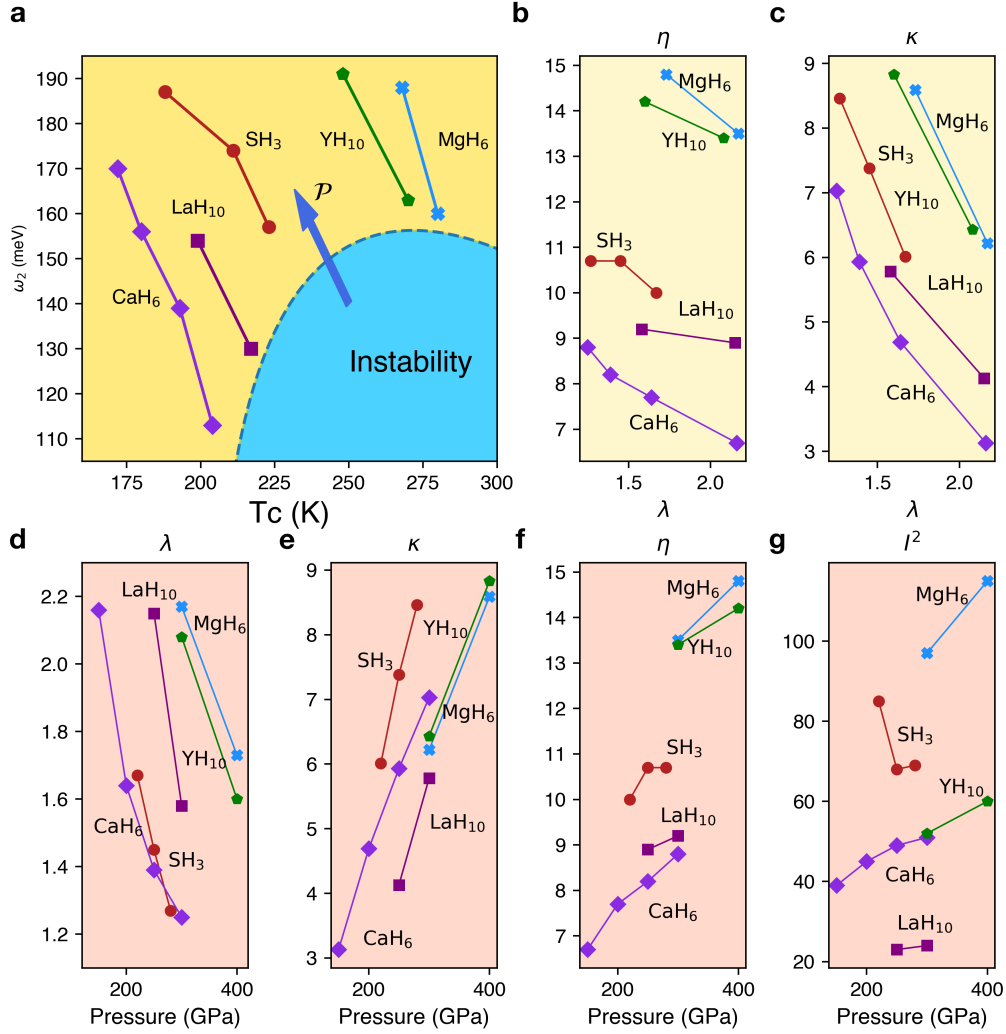
FIG. 2: Interrelationships between the various materials characteristics for the H atoms in the hydrides we discuss. (a) Schematic $\omega_2 - T_c$ phase diagram, with blue indicating the island of lattice instability. The blue arrow denotes the direction of increasing pressure (P). (b),(c) Plots of κ and η respectively, versus $\lambda = \frac{\eta}{\kappa}$. Increase of λ correlates strongly with decrease in κ (frequencies). (d),(e),(f),(g) Plots of λ. $\kappa = M\omega_2^2$ (eV/Å^2), $\eta = N(0)I^2$ (eV/Å^2), and I^2 (eV^2/Å)^2, respectively, versus pressure. All panels show each of the five hydrides toward the lower end of their region of stability.

butions alone: unless otherwise stated (sometimes the H subscript is included for emphasis), our comments apply only to the H atoms' contributions (the rows in the tables in the Appendix labeled "H"). The following observations are drawn from the $\omega_2 - T_c$ phase diagram and six other panels providing a variety of correlations in Fig. 2.

1. High frequencies but not too high

Higher T_c compounds have higher frequency moments, compare Fig. 2(a) with Fig. 2(e). Figure 2(a) provides an ω_2 vs. T_c phase diagram, which identifies a boundary separating the high T_c region from an island of lattice instability. Interestingly, MgH$_6$ at the highest T_c end has very similar
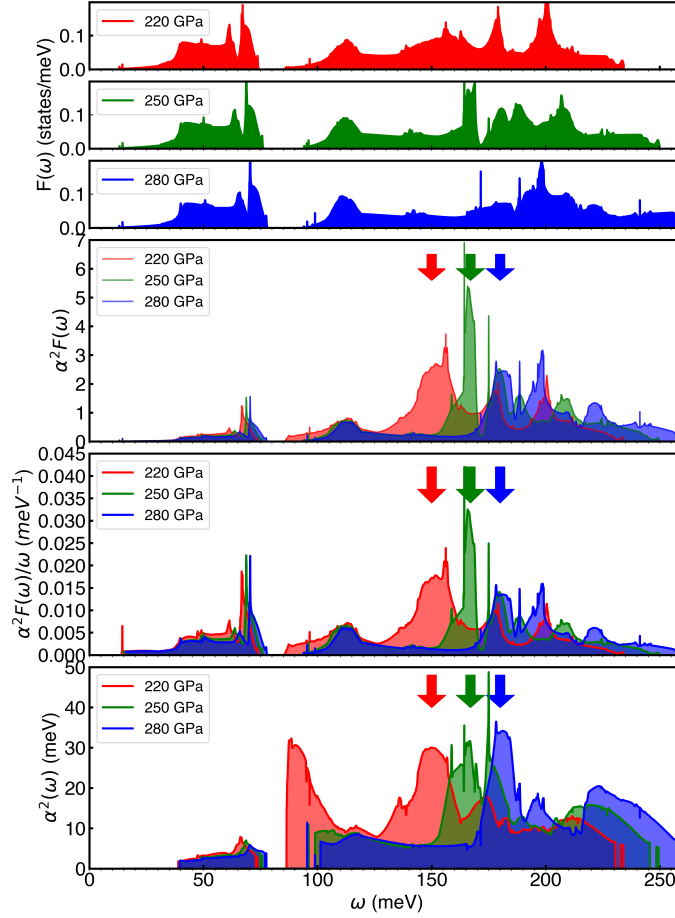
5

FIG. 3: Views of the evolution under pressure of phonon coupling strength and frequencies for SH_3. From top: $F(\omega)$ for the three pressures indicated; the Eliashberg function $\alpha^2 F(\omega)$; the ratio $\alpha^2 F(\omega)/\omega$ that determines λ and frequency moments; the coupling spectrum $\alpha^2(\omega)$. Note that in these zone-averaged functions there is no indication of the lattice instability that occurs just below 200 GPa.

frequencies as SH_3. Since the denominator $M_H \omega_2^2$ in λ is the same for these two materials, the numerator η must be substantially larger. Figure 2(f) and the tables in the Appendix indeed show that η is $\sim 35\%$ larger, with *twice as large matrix elements* I_H^2 [Fig. 2(g)] overcoming a somewhat lower value of $N(0)$. This is the first clear evidence of a strong material dependence of I_H^2 in hydrides.

2. Highest T_c lies at low frequency end

Since pressure enhancement of hydride T_c has been a prevalent notion, we quantify that T_c *de-creases with increasing pressure and increasing fre-quencies* within each class studied. Strong coupling is (unfortunately) associated with lower frequencies, within a region of stability. This result (noted previously in some individual materials) seems in opposition to conventional wisdom that higher pressure is better for T_c. Our results establish that T_c is maximum at the lower pressure end of crystal stability where frequencies are softer, as shown in Fig. 2(a). T_c is ultimately limited in these systems, as in many strong coupled but lower T_c analogues, by lattice instability[45–47] that depends on the details of EPC of the material. The emerging picture is that while pressure stabilizes

favorable structures with metallic *atomic H*, providing high T_c with high frequencies, *within each phase* additional pressure increases frequencies but lowers λ_H and T_c. To repeat: the essential role of pressure is simply to stabilize structures composed of atomic H; further pressure is detrimental for T_c. Less pressure, that is, the instability region, comprises insulating phases with H_2 and H^- units, or conducting structures with these units,[48] which do not promote strong scattering and strong EPC.

3. H matrix elements are not "atomic properties"

The derived squared H matrix element I_H^2 has been suggested to be an "atomic quantity,"[32, 49] not varying much from material to material. I_H^2 is highlighted in boldface in Tables I-III of the Appendix and plotted versus pressure in Fig. 2(g), facilitating observing that it differs by a *factor of five* for these compounds: 24 for LaH_{10} to 125 in MgH_6, each in $eV^2/Å^2$. Evidently the screening of the proton displacement is sensitive to the response of the environment, and I_H^2 is not the "atomic quantity" as earlier suggested.

4. Impact of atomic fraction of H

Is the atomic fraction of H a crucial factor? By dividing $N_H(0)$ in the tables in the Appendix by the number of H atoms, the contribution per H atom is obtained. The values range from around 0.022 for CaH_6 and MgH_6 to 0.033 for the vHs compounds SH_3, LaH_{10}, and YH_{10}; units are states/(eV atom spin). These values, which represent chemical differences and can be sensitive to the precision of the calculation and to decompositions into X and H contributions, do not scale well with T_c.

5. Behavior of λ(P)

The variation of λ with pressure depends primarily on the strong variation with pressure of the lattice stiffness $\kappa = M\omega_2^2$, see Fig. 2(c). For example, κ decreases by 55% in CaH_6 from 300 to 150 GPa, beyond which the lattice becomes unstable. The minor variation of the electronic stiffness $\eta = N(0)I^2$ is apparent from Fig. 2 (f). Increasing

λ by softening the lattice increases T_c for currently studied hydrides but encounters lattice instability for $\lambda_H \approx 2.2$.

6. Achievement of "atomic hydrogen"

These alkaline earth and rare earth based compounds are effectively atomic hydrogen crystals with a charge carrier void (more precisely, a scattering strength void) in the volume consumed by the X atom: the X atom serves to compress and to provide electrons to destabilize H_2 units and produce atomic (versus diatomic) H, thereby enhancing scattering and producing HTS. This observation suggests that element(s) X that are most able to "break" H_2 molecules into atoms in a crystalline environment provide the most promise of providing Ashcroft's "chemical precompression concept,"[49] *i.e.* decreasing the pressure necessary to obtain HTS hydrides.

V. PROSPECTS FOR HIGHER T_c, AND LIMITATIONS

We collect here some important characteristics, by example from the various compounds.
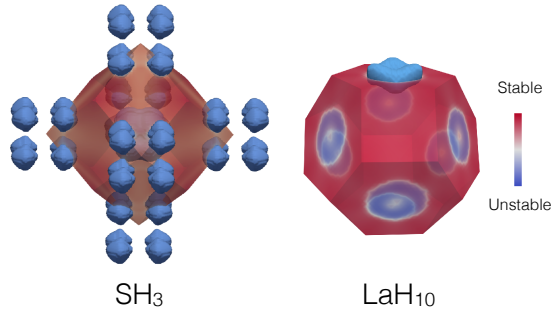

FIG. 4: Regions of unstable phonons. The indicated regions of the Brillouin zone indicate where phonons first becomes unstable, in harmonic approximation. For SH_3 the instability regions are repeated outside the first zone for more clarity.

A. Strong coupling and lattice instability

There have been many examples over several decades[45–47] where pushing a superconducting system toward stronger coupling results in marginally higher T_c, accompanied by renormalization toward softer phonons followed by lattice instability. The process is understood: EPC renormalizes phonon frequencies ω_q downward from their bare values Ω_q:

$$\omega_q^2 = \Omega_q^2 - 2\Omega_q\Pi_q(\omega_q) \qquad (4)$$

where $\Pi_q(\omega)$ is the phonon self-energy that increases with λ_q: increasing coupling drives frequencies downward, as seen from the tables in the Appendix. Then, lower frequencies increase the coupling strength measured by λ (other things being equal): it is a cooperative process inviting vanishing frequencies and the accompanying lattice instability and material-dependent limitation of T_c.

The process is illustrated for SH_3 in Fig. 3, where $F(\omega), \alpha^2 F(\omega), \alpha^2 F(\omega)/\omega$, and $\alpha^2(\omega)$ are shown for a range of (harmonic) lattice stability above the instability around 140 GPa, from which distinct features can be identified. The differences with pressure in $F(\omega)$ are unexceptional, with some hardening of the high frequency H modes proceeding as expected. Differences in $\alpha^2 F$ begin to be more evident: peak values decrease from 170 to 150 to 130 meV as pressure is *lowered*. This shift downward of coupling strength is more striking in $\alpha^2(\omega) = \alpha^2 F(\omega)/F(\omega)$, which reveals very strong coupling in the 80-120 meV region. These H-derived optic modes are reflected in the moments of $\alpha^2 F$ in Tables in the Appendix: ω_2 decreases by a third before instability. Neither the moments – *e.g.* ω_{log}, which probably (over)emphasizes the low frequency modes – nor λ dictates the instability of the lattice by vanishing or diverging, respectively.

Instead, a single branch (with small phase space) dips toward zero and the structure becomes dynamically unstable. In these hydrides the lower pressure, roomier structures tend to allow molecular-like dimerization of some of the H atoms into H_2 units, which is unfavorable for metallicity and strong coupling. Figure 4 indicates the regions of the zone where instabilities in SH_3 and LaH_{10} occur. In HS_3 the instability lies along the H-P symmetry line along the zone boundary, with another instability occurring at Γ. In LaH_{10} the instabilities occur in a donut shape centered on the

L point. In both cases as well as in CaH_6, the instability involves wavevectors at or near the zone boundaries, with the short wavelengths being suggestive of the instabilities being related to H_2 unit type fluctuation and formation.

B. Highest T_c class: rare earth decahydrides $X\mathbf{H}_{10}$

A noteworthy feature is that, for LaH_{10} as in SH_3 which are the two materials so far observed to be superconducting nearing room temperature, the Fermi level accidentally (if it is accidental) falls between the energies of a pair of closely spaced van Hove singularities (vHs). The associated pieces of Fermi surface in LaH_{10} and resulting vHs peak in $N(E)$ involve *solely* the H8 site, see Fig. 1. The additional physics[15] occurring in SH_3 due to vHs will also apply to LaH_{10} (but in less prominent form), but that is not the topic of this paper. The variation of $N(E)$ from 210 GPa to 300 GPa, is regular but minor, and the changes in Fermi surface are not visible in surface plots. YH_{10} has a predicted T_c=250-270K compared to LaH_{10} at 200-215K. The values of λ at the two pressures studied are the same; the difference lies in the $\sim 40\%$ higher value of $\eta = N(0)I^2$ in YH_{10}, where a *much larger value of I^2* overcomes a somewhat lower value of $N(0)$. Based on current examples, increasing λ near the instability by phonon softening does increase T_c but also drives the instability, a familiar story from 1970s materials.

C. Variations within a class: alkaline earth hexahydrides $X\mathbf{H}_6$

Metal hexahydrides have been predicted to include high T_c superconductors at high pressure, but synthesis and study of their properties have not yet been reported. Given the regularities discussed above, it is eye-opening to note that both the lowest and the highest T_c members in Fig. 2 are CaH_6 and MgH_6 respectively, despite being isostructural, isovalent, and in neighboring rows in the periodic table. The difference, surprisingly, is not in higher frequencies in the smaller cell (the frequencies are similar) but in the matrix elements I_H^2. The origin of this difference is a topic of on-
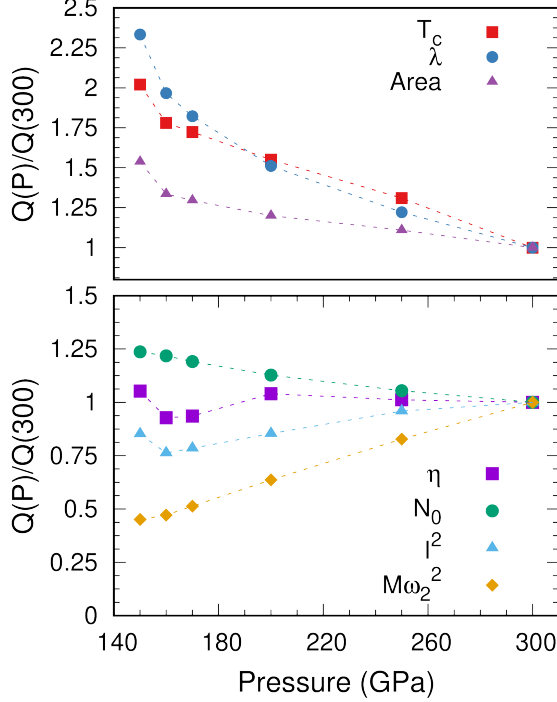
going study for us.

FIG. 5: Pressure dependence of various superconducting quantities of cubic CaH_6. A denotes the area under $\alpha^2 F$, see the text. All quantities refer to the hydrogen contribution alone. As emphasized in the main text, λ and T_c increase (rather strongly) at the low pressure end, before the instability. The lower panel shows that the decrease of ω_2^2 is responsible, even though from frequency moments no impending instability can be inferred, For this data, norm conserving pseudopotentials were used.

A plot of the H-related parameters for CaH_6 at 150-300 GPa in Fig. 5, normalized to their values at 300 GPa, illuminate relative increases and decreases with pressure. The main trends follow those of SH_3: T_c is highest at the lower pressure, with a quick upturn in λ and T_c just before the lattice becomes unstable. For this structure as for others: once the structure becomes stable, $T_c(P)$ *decreases* with increasing pressure, by up to a factor of two in our range of study.

VI.   QUANTITIES DESERVING OF FOCUS

A. η_H versus κ_H

The hydrides studied here reach their maximum T_c, just before instability, near a common value $\lambda_H \approx 2.2$ (somewhat smaller in SH_3), while T_c varies from 200K to 285K. The distinction is that those with higher mean frequency just above the instability have the higher T_c. At first glance, the goal should be to retain strong coupling at the higher frequencies; for room temperature T_c Bergmann and Rainer's analysis[41] suggests that for a 300K superconductor, coupling at $2\pi k_B T_c$=165 meV and above is optimal; this is in the range of the mean frequencies of the highest T_c hydrides (see tables in the Appendix).

This choice of goal is somewhat simplistic, however, because (i) high mean frequencies reduce λ (see Eq. (1)), and (ii) the strongly coupled low frequency modes are in the lower frequency (not optimal frequency) range and are approaching instability precisely because they are the most strongly coupled (a chicken and egg relationship). This is the limitation that has persisted for five decades: stronger coupling inches T_c upward but enforces lattice instability. The best strategy seems to be to (somehow) retain strong coupling as evenly as possible over all H vibrations, preferably utilizing all momenta. Such a scenario postpones a lattice instability until a large fraction of modes become soft.

This brings consideration to the McMillan-Hopfield constant $\eta_H = N_H(0)I_H^2$, which the analysis of Allen and Dynes indicates as the limiting behavior of T_c at large coupling. Fig. 2(f) shows that η_H is much larger for the higher T_c materials (LaH_{10} is an exception). The next challenge therefore is to engineer η_H because (i) so little is known about how to maximize the matrix elements I^2, and (ii) $N(0)$ can be sensitive to details of band structure that simply has to be calculated. Gaining an understanding of H scattering I_H^2 is a current challenge but a realistic one, and one that will be crucial in learning how to retain coupling over as many H branches as possible.
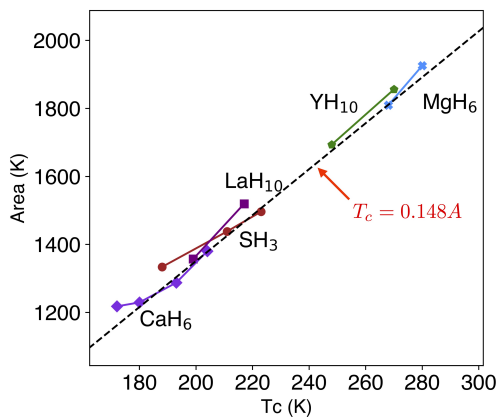
9

FIG. 6: Plot of area under $\alpha^2 F_H$ (the H contribution) versus T_c, for binary hydrides, using H-derived quantities. The slope 0.148 denotes the Leavens-Carbotte line for strong coupled superconductors existing in 1974.

B. Leavens-Carbotte analysis

An understanding of how to increase T_c requires one to internalize the actual factors that determine T_c in the current regime of coupling and T_c, which is not yet at all in the strong coupling limit. In this respect: the somewhat involved Allen-Dynes expression is opaque – despite its appearance, it is not exponential except near $T_c=0$ where it was never intended to be used. Leavens and Carbotte found for strong coupling materials of the time (1974) [50] that the area A under $\alpha^2 F$, which from the various definitions is $A = \lambda\omega_1/2$, was a faithful indicator of T_c: $T_c \approx 0.148A$.

Using our H-based (not total) values of A and T_c, their relationship is presented in Fig. 6, along with the Leavens and Carbotte slope of 0.148. The agreement for these five hydrides is stunningly close to their value; a least squares fit to $T_c=S\,A +T_o$ gives a practically equivalent slope of $S=0.150$ and a small intercept of $T_o=-6K$ – a *direct linear relationship* to within computational uncertainty. This relationship focuses the challenge: maximize the product $\lambda\omega_1 \propto \eta_H/ <\omega_H>$. Allen and Dynes proved that the strong coupling (large λ) limit of Eliashberg theory is $T_c \propto \omega_2\sqrt{\lambda} = \eta/M$. Note: the difference between ω_1 and ω_2 in these hydrides is nearly a constant ratio, so for consideration of these limits they may be considered to be interchangeable. Thus the strong coupling regime in hydrides has not been approached, and the Leavens-Carbotte quantity A provides the quantity to increase.

Our work provides another guide for reducing the pressure required for HTS hydrides. One objective is to find the element(s) X in XH_n that serves to disassociate the H_2 unit into atomic H in the lattice at the lowest possible pressure – not a really new observation, but also not one with any underlying understanding. Many examples indicate that a high T_c phase is then likely to emerge. Our view then is that the optimum set of materials parameters, for higher T_c possibly at lower pressures, is yet to be achieved.

VII. ACKNOWLEDGMENTS

Appendix A: Material parameters from separation of atomic contributions

Tables I-III provide the extensive numerical data calculated for the five hydrides in the three crystal structure classes that we have studied. The rows follow the separation of the various quantities into metal atom (S, Ca, Mg, La, Y), hydrogen (H), and total (T) compound values (the latter where appropriate). Procedures are described in the main text.

10

	$\mathcal{P}$		ω_{log}	ω_1	ω_2	$N_{\uparrow}(0)$	I^2	η	$M\omega_2^2$	A	λ	T_c
	GPa		meV	meV	meV	$\frac{1}{eV}$	$\frac{eV^2}{\mathring{A}^2}$	$\frac{eV}{\mathring{A}^2}$	$\frac{eV}{\mathring{A}^2}$	meV		K
		S	51	53	55	0.12	85	9.8	24.0	11	0.41	1
	220	H	151	155	158	0.13	**79**	10.1	6.1	128	1.66	222
		T	122	135	144	0.24	-	-	5.0	140	2.08	229
		S	52	55	57	0.14	67	9.4	25.5	10	0.37	0
SH_3	250	H	167	171	174	0.15	**71**	10.7	7.4	124	1.45	211
		T	132	147	157	0.29	-	-	6.0	134	1.82	218
		S	52	55	58	0.14	61	8.9	26.1	9	0.34	0
	280	H	178	182	186	0.15	**69**	10.7	8.4	115	1.27	189
		T	137	155	167	0.30	-	-	6.8	125	1.61	199

TABLE I: Various computed properties related to superconductivity of SH_3, separated into contributions from the sulfur (S) and hydrogen (H) atoms separately, as well as the total. Other XH$_3$ compounds with the same structure have been predicted to be less promising as high temperature superconductors. I^2 and η are atomic quantities, not defined for generic compounds. Certain H quantities have been emphasized in boldface font. Note the small variation in η with pressure, and that the frequency moments scale together well.

	$\mathcal{P}$		ω_{log}	ω_1	ω_2	$N_{\uparrow}(0)$	I^2	η	$M\omega_2^2$	A	λ	T_c
	GPa		meV	meV	meV	$1/eV$	$\frac{eV^2}{\mathring{A}^2}$	$\frac{eV}{\mathring{A}^2}$	$\frac{eV}{\mathring{A}^2}$	meV		K
		Ca	31	32	33	0.01	...	4.0	10.7	6	0.37	0
	150	H	108	110	113	0.17	**39**	6.7	3.1	119	2.16	204
		T	90	99	105	0.17	-	-	2.7	125	2.53	200
		Ca	34	35	36	0.01	...	4.2	13.2	5	0.32	0
	200	H	134	136	139	0.17	**45**	7.7	4.7	111	1.64	193
		T	107	120	128	0.17	-	-	4.0	117	1.95	190
CaH_6		Ca	37	38	39	0.01	...	4.7	15.4	5	0.30	0
	250	H	151	153	156	0.17	**49**	8.2	5.9	106	1.39	180
		T	117	133	142	0.17	-	-	4.9	112	1.69	180
		Ca	39	40	42	0.01	...	5.8	17.1	6	0.34	0
	300	H	165	168	170	0.13	**51**	8.8	7.0	105	1.25	172
		T	122	141	152	0.18	-	-	5.6	111	1.59	175
		Mg	48	49	50	0.04	128	5.6	15.1	9	0.37	0
	300	H	146	153	160	0.14	**97**	13.5	6.2	166	2.17	280
MgH_6		T	124	138	149	0.18	-	-	5.4	175	2.54	279
		Mg	53	54	55	0.04	121	4.8	18.1	7	0.27	0
	400	H	174	181	188	0.13	**115**	14.8	8.6	156	1.73	268
		T	149	164	176	0.17	-	-	7.5	163	2.00	269

TABLE II: Contributions for CaH$_6$ and MgH$_6$ of the metal and H atoms separately (see main text), as well as the total (T) value, to the parameters determining T$_c$. The I^2 values for CaH$_6$ are not presented because the Ca density of states needed to derive them are too small and uncertain to obtain reliable values.

	$\mathcal{P}$		ω_{log}	ω_1	ω_2	$N_\uparrow(0)$	I^2	η	$M\omega_2^2$	A	λ	T_c
	GPa		meV	meV	meV	$\frac{1}{eV}$	$\frac{eV^2}{\mathring{A}^2}$	$\frac{eV}{\mathring{A}^2}$	$\frac{eV}{\mathring{A}^2}$	meV		K
		La	23	24	25	0.07	98	6.5	21.2	3	0.31	0
	250	H	112	121	130	0.38	**23**	8.9	4.1	131	2.15	217
LaH_{10}		T	92	109	122	0.44	-	-	3.6	134	2.46	206
		La	24	25	26	0.07	77	5.1	24.0	2	0.21	0
	300	H	141	148	154	0.37	**24**	9.2	5.8	117	1.58	199
		T	115	133	145	0.43	-	-	5.1	120	1.80	189
		Y	24	25	26	0.11	44	5.0	14.6	4	0.34	0
	300	H	145	154	163	0.25	**52**	13.4	6.4	160	2.08	270
YH_{10}		T	113	136	151	0.36	-	-	5.5	165	2.42	249
		Y	30	30	31	0.11	41	4.4	21.3	3	0.21	0
	400	H	174	183	191	0.23	**60**	14.2	8.8	146	1.60	248
		T	142	165	180	0.34	-	-	7.9	149	1.81	236

TABLE III: Various computed properties related to superconductivity for LaH_{10} and YH_{10} of the metal and H atoms separately (see main text), as well as the total (T) value, to the parameters determining T_c.

[1] D. Duan, Y. Liu, F. Tian, D. Li, X. Huang, Z. Zhao, H. Yu, B. Liu, W. Tian, T. Cui, Pressure-induced metalization of dense $(H_2S)_2H_2$ with high-T_c superconductivity, Sci. Rep. **4**, 6968 (2014).

[2] A. P. Drozdov, M. I. Eremets, I. A. Troyan, V. Ksenofontov, S. I. Shylin, Conventional superconductivity at 203 kelvin at high pressures in the sulfur hydride system, Nature **525**, 73 (2015).

[3] M. Einaga, M. Sakata, T. Ishikawa, K. Shimizu, M. I. Eremets, A. P. Drozdov, I. A. Troyan, N. Hirao, Y. Ohishi, Crystal structure of the superconducting phase of sulfur hydride, Nature Physics **12**, 835 (2016).

[4] D. Duan, Y. Liu, Y. Ma, Z. Shao, B. Liu, T. Cui, Structure and superconductivity of hydrides at high pressure, Natl. Sci. Rev. **4**, 121 (2017).

[5] A. P. Drozdov, V. S. Minkov, S. P. Besedin, P. P. Kong, M. A. Kuzovnikov, D. A. Knyazev, M. I. Eremets, Superconductivity at 215 K in lanthanum hydride at high pressures, arXiv:1808.07039.

[6] M. Somayazulu, M. Ahart, A. K Mishra, Z. M. Geballe, M. Baldini, Y. Meng, V. V. Struzhkin, R. J. Hemley, Evidence for superconductivity above 260 K in lanthanum superhydride at megabar pressures, Phys. Rev. Lett. **122**, 027001 (2019).

[7] A. P. Drozdov, P. P. Kong, V. S. Minkov, S. P. Besedin, M. A. Kuzovnikov, S. Mozaffari, L. Balicas, F. Balakirev, D. Graf, V. P. Prakapenka, E. Greenberg, D. A. Knyazev, M. Tkacz, M. I. Eremets, Superconductivity at 250 K in lanthanum hydride under high pressures, Nature **569**, 528 (2019).

[8] P. P. Kong *et al.*, Superconductivity up to 243K in yttrium hydrides under high pressure, arXiv:1909.10482.

[9] Y. Li, J. Hao, H. Liu, Y. Li, Y. Ma, The metallization and superconductivity of dense hydrogen sulfide, J. Chem. Phys. **140**, 174712 (2014).

[10] D. A. Papaconstantopoulos, B. M. Klein, M. J. Mehl, W. E. Pickett. Cubic H_3S around 200 GPa: an atomic hydrogen superconductor stabilized by sulfur, Phys. Rev. B **91**, 184511 (2015).

[11] I. Errea, M. Calandra, C. J. Pickard, J. Nelson, R. J. Needs, Y. Li, H. Liu, Y. Zhang, Y. Ma, F. Mauri, High-pressure hydrogen sulfide from first principles: a strongly anharmonic phonon-mediated superconductor, Phys. Rev. Lett. **114**, 157004, (2015).

[12] J. A. Flores-Livas, A. Sanna, E. K. U. Gross, High temperature superconductivity in sulfur and selenium hydrides at high pressure, Eur. Phys. J. B **89**, 63 (2016).

[13] N. Bernstein, C. S. Hellberg, M. D. Johannes, I. I. Mazin, M. J. Mehl, What superconducts in sulfur hydrides under pressure and why, Phys. Rev. B **91**, 060511(R) (2015).

[14] R. Akashi, M. Kawamura, S. Tsuneyuki, Y. Nomura, R. Arita, First-principles study of the pressure and crystal-structure dependences of the superconducting transition temperature in compressed sulfur hydrides, Phys. Rev. B **91**, 224513 (2015).

[15] Y. Quan and W. E. Pickett, van Hove singularities and spectral smearing in high temperature superconducting H_3S, Phys. Rev. B **93**, 104526 (2016).

[16] X. Zhong, H. Wang, J. Zhang, H. Liu, S. Zhang, H. Song, G. Yang, L. Zhang, and Y. Ma, Tellurium hydrides at high pressures: high-temperature superconductors, Phys. Rev. Lett. **116**, 057002 (2016).

[17] F. Peng, Y. Sun, C. J. Pickard, R. J. Needs, Q. Wu, Y. Ma, Hydrogen clathrate structures in rare earth hydrides at high pressures: possible route to room-temperature superconductivity, Phys. Rev. Lett. **119**, 107001 (2017).

[18] H. Liu, I. I. Naumov, R. Hoffmann, N. W. Ashcroft, R. J. Hemley, Potential high-Tc superconducting lanthanum and yttrium hydrides at high pressure, Proc. Natl. Acad. Sci. bf 114, 6990 (2017).

[19] T. Bi, N. Zarifi, T. Terpstra, E. Zurek, The search for superconductivity in high pressure hydrides, Reference Module in Chemistry, Molecular Sciences, and Chemical Engineering, arXiv:1806.00163. https://doi.org/10.1016/B978-0-12-409547-2.11435-0

[20] E. Zurek and T. Bi, High-temperature superconductivity in alkaline and rare earth polyhydrides at high pressure: a theoretical perspective, J. Chem. Phys. **150**, 050901 (2018).

[21] X. Feng, J. Zhang, G. Gao, H. Liu, and H. Wang, Compressed sodalite-like MgH_6 as a potential high-temperature superconductor, RSC Adv. **5**, 59292 (2015).

[22] H. Wang, J. S. Tse, K. Tanaka, T. Iitaka, and Y. Ma, Superconductive sodalite-like clathrate calcium hydride at high pressures, Proc. Natl. Acad. Sci. U.S.A. **109**, 6463 (2012).

[23] D. V. Semenok, A. G. Kvashnin, A. G. Ivanova, V. Svitlyk, I. A. Troyan, and A. R. Oganov, Synthesis of ThH_4, ThH_6, ThH_9 and ThH_{10}: a route to room-temperature superconductivity, arXiv:1902.10206.

[24] P. B. Allen, R. C. Dynes, Transition temperature of strong-coupled superconductors reanalyzed, Phys. Rev. B **12**, 905 (1975).

[25] See Supplemental Material at [URL will be inserted by publisher] for structural data for the compounds we have studied (Sec. I), the full experssion for the Allen-Dynes equation for T_c (Sec. II), our constant $\alpha^2 F$ model that allows extraction of the parameters discussed in the text from published curves of $\alpha^2 F$ (Secs. III and IV), and additional plots from somewhat different viewpoints analogous to Fig. 2(a) in the main text (Sec. V).

[26] F. Giustino, Electron-phonon interactions from first principles, Rev. Mod. Phys. **89**, 015003 (2017).

[27] J. A. Flores-Livas, L. Boeri, A. Sanna, G. Profeta, R. Arita, and M. Eremets, A Perspective on Conventional High-Temperture Superconductors at High Pressure: Methods and Materials, arXiv:1905.06693.

[28] G. Gaspari and B. L. Györffy, Electron-phonon interactions, d resonances, and superconductivity in transition metals, Phys. Rev. Lett. **28**, 801 (1972).

[29] D. A. Papaconstantopoulos, L. L. Boyer, B. M. Klein, A. R. Williams, V. L. Morruzzi, and J. F. Janak, Calculations of the superconnducting properties of 32 metals with Z<49, Phys. Rev. B **15**, 4221 (1977).

[30] W. E. Pickett, Transferability and the Electron-Phonon Interaction: A Reinterpretation of the-Rigid Muffin-Tin Approximation, Phys. Rev. B **25**, 745 (1982).

[31] W. L. McMillan, Transition temperature of strong-coupled superconductors, Phys. Rev. B **167**, 331 (1968).

[32] J. J. Hopfield, Angular momentum and transition-metal superconductivity, Phys. Rev. **168**, 443 (1969).

[33] P. Giannozzi, O. Andreussi, T. Brumme, O. Bunau, M. Buongiorno Nardelli, M. Calandra, R. Car, C. Cavazzoni, D. Ceresoli, M. Cococcioni, N. Colonna, I. Carnimeo, A. Dal Corso, S. de. Gironcoli, P. Delugas, R. A. DiStasio Jr, A. Ferretti, A. Floris, G. Fratesi, G. Fugallo, R. Gebauer, U. Gerstmann, F. Giustino, T. Gorni, J. Jia, M. Kawamura, H-Y Ko, A. Kokalj, E. Kkbenli, M. Lazzeri, M. Marsili, N. Marzari, F. Mauri, N. L Nguyen, H-V Nguyen, A. Otero de-la Roza, L. Paulatto, S. Ponc, D. Rocca, R. Sabatini, B. Santra, A. P. Seitsonen, A. Smogunov, I. Timrov, T. Thonhauser, P. Umari, N. Vast, X. Wu, S. Baroni, Advanced capabilities for materials modelling with QUANTUM ESPRESSO, *J. Phys.: Condensed Matter* **29**, 465901 (2017).

[34] D. R. Hamann, Optimized norm-conserving Vanderbilt pseudopotentials, Phys. Rev. B **88**, 085117 (2013).

[35] J. P. Perdew, K. Burke, M. Ernzerhof, Generalized gradient approximation made simple, Phys. Rev. Lett. **77**, 3865 (1996).

[36] M. Kawamura, Y. Gohda, S. Tsuneyuki, Improved tetrahedron method for the Brillouin-zone integration applicable to response functions, Phys. Rev. B **89**, 094515 (2014).

[37] I. Errea *et al.*, Quantum crystal structure in the 250K superconducting lanthanum hydride, arXiv:1907.11916.

[38] I. Errea, M. Calandra, C. J. Pickard, J. R. Nelson, R. J. Needs, Y. Li, H. Liu, Y. Zhang, Y. Ma, and F. Mauri, Quantum hydrogen bond symmetrization in the superconducting hydrogen sulfide system, Nature **533**, 81 (2016).

[39] S. Poncé, E.R. Margine, C. Verdi, F. Giustino, EPW: Electron-phonon coupling, transport and superconducting properties using maximally localized Wannier functions, Comp. Phys. Comm. **209**, 116 (2016).

[40] A. A. Mostofi, J. R. Yates, Y.-S. Lee, I. Souza, D. Vanderbilt, N. Marzari, wannier90: a tool for obtaining maximally-localised Wannier functions, Comp. Phys. Comm. **178**, 685 (2008).

[41] G. Bergmann, D. Rainer, The sensitivity of the transition temperature to changes in $\alpha^2 F(\omega)$, Z. f. Physik **263**, 59 (1973).

[42] P. B. Allen and M. L. Cohen, Superconductivity and phonon softening, Phys. Rev. Lett. **29**, 1593(1972).

[43] P. B. Allen, Neutron spectroscopy of superconductors, Phys. Rev. B **6**, 2577 (1972).

[44] W. E. Pickett, The next breakthrough in phonon-mediated superconductivity, Physica C **468**, 126 (2008).

[45] W. Weber, Phonon anomalies in strongly coupled superconductors, Phys. Rev. B **8**, 5093 (1973).

[46] L. R. Testardi, Structural instability and superconductivity in A-15 compounds, Rev. Mod. Phys. **47**, 637 (1975).

[47] W. E. Pickett, Design for a room temperature superconductor. J. Supercond. & Novel Magn. **19**, 291 (2006).

[48] T. Bi, N. Zarifi, T. Terpstra, E. Zurek, The Search fo Superconductivity in High Pressure Hydrides, in *Ref. Module in Chemistry, Molecular Sciences, and Chemical Engineering* (2019); arXiv:1806.00163;doi.org/10.1016/B978-0-12-409547-2.11435-0.

[49] N. W. Ashcroft, Hydrogen Dominant Metallic Alloys: High Temperature Superconductors? Phys. Rev. Lett. **92**, 187002 (2004).

[50] C. R. Leavens and J. P. Carbotte, An important parameter in high-temperature superconductivity, J. Low Temp. Phys. **14**, 195 (1974).